Article

Down Syndrome Developmental Brain Transcriptome Reveals Defective Oligodendrocyte Differentiation and Myelination

Highlights

- Genome-wide spatiotemporal dysregulation of gene expression is found in DS brains

- Transcriptome changes reflect altered oligodendrocyte development and myelination

- Oligodendrocyte differentiation and myelination is altered in DS model mice (Ts65Dn)

- Speed of action potential propagation is decreased in Ts65Dn neocortical white matter

Authors

Jose Luis Olmos-Serrano,
Hyo Jung Kang, William A. Tyler, ...,
Jeffrey A. Golden, Tarik F. Haydar,
Nenad Sestan

Correspondence

thaydar@bu.edu (T.F.H.),
nenad.sestan@yale.edu (N.S.)

In Brief

Olmos-Serrano et al. identify defects in oligodendrocyte differentiation and white matter development over the timespan in Down syndrome (DS) brain and in Ts65Dn trisomic mice. Their developmental gene expression study provides a new framework for investigating DS neuropathogenesis.

Accession Numbers

GSE59630

CrossMark

CellPress

CellPress

Down Syndrome Developmental Brain Transcriptome Reveals Defective Oligodendrocyte Differentiation and Myelination

Jose Luis Olmos-Serrano,[1,9] Hyo Jung Kang,[2,3,9] William A. Tyler,[1,9] John C. Silbereis,[2,9] Feng Cheng,[2,4] Ying Zhu,[2] Mihovil Pletikos,[2] Lucija Jankovic-Rapan,[2] Nathan P. Cramer,[5] Zygmunt Galdzicki,[5] Joseph Goodliffe,[1] Alan Peters,[1] Claire Sethares,[1] Ivana Delalle,[6] Jeffrey A. Golden,[7] Tarik F. Haydar,[1,*] and Nenad Sestan[2,8,*]

[1]Department of Anatomy and Neurobiology, Boston University School of Medicine, Boston, MA 02118, USA
[2]Department of Neuroscience and Kavli Institute for Neuroscience, Yale School of Medicine, New Haven, CT 06510, USA
[3]Department of Life Science, Chung-Ang University, Seoul 06974, Korea
[4]Department of Pharmaceutical Sciences, College of Pharmacy, University of South Florida, Tampa, FL 33620, USA
[5]Department of Anatomy, Physiology, and Genetics, F. Edward Hébert School of Medicine, Uniformed Services University of the Health Sciences, Bethesda, MD 20814, USA
[6]Department of Pathology and Laboratory Medicine, Boston University School of Medicine, Boston, MA 02118, USA
[7]Department of Pathology, Brigham and Women's Hospital, Boston, MA 02115, USA
[8]Departments of Genetics and Psychiatry, Section of Comparative Medicine, Program in Cellular Neuroscience, Neurodegeneration and Repair, Child Study Center, Yale School of Medicine, New Haven, CT 06510, USA
[9]Co-first author
*Correspondence: thaydar@bu.edu (T.F.H.), nenad.sestan@yale.edu (N.S.)
http://dx.doi.org/10.1016/j.neuron.2016.01.042

SUMMARY

Trisomy 21, or Down syndrome (DS), is the most common genetic cause of developmental delay and intellectual disability. To gain insight into the underlying molecular and cellular pathogenesis, we conducted a multi-region transcriptome analysis of DS and euploid control brains spanning from mid-fetal development to adulthood. We found genome-wide alterations in the expression of a large number of genes, many of which exhibited temporal and spatial specificity and were associated with distinct biological processes. In particular, we uncovered co-dysregulation of genes associated with oligodendrocyte differentiation and myelination that were validated via cross-species comparison to Ts65Dn trisomy mice. Furthermore, we show that hypomyelination present in Ts65Dn mice is in part due to cell-autonomous effects of trisomy on oligodendrocyte differentiation and results in slower neocortical action potential transmission. Together, these results identify defects in white matter development and function in DS, and they provide a transcriptional framework for further investigating DS neuropathogenesis.

INTRODUCTION

Trisomy for human chromosome 21 (HSA21) causes Down syndrome (DS) in one of every 732 live births (Canfield et al., 2006), making it the most common genetic cause of developmental delay and intellectual disability. DS is characterized by a constel-

lation of phenotypes affecting many organ systems, including CNS abnormalities such as cognitive and motor impairments, microcephaly, and the early appearance of neuropathological characteristics of Alzheimer's disease (AD; Hartley et al., 2015; Haydar and Reeves, 2012; Letourneau et al., 2014; Lott, 2012).

Prior insights into DS neuropathology have come from studies of human individuals and trisomic mouse models. Morphometric and cellular studies on human brain indicate that trisomy 21 causes complex spatiotemporal disturbances in neural development (Golden and Hyman, 1994; Larsen et al., 2008; Haydar and Reeves, 2012). Mouse models have provided additional insights into the developmental progression of DS, elucidating specific defects in neurogenesis, neuronal differentiation, and impaired synaptic plasticity and learning (Chakrabarti et al., 2007, 2010; Cramer et al., 2015; Hyde et al., 2001; Kleschevnikov et al., 2004; Siarey et al., 1997, 1999; Tyler and Haydar, 2013; Wang et al., 2013). While it is clear that trisomy of HSA21 is the root cause of DS, which biological processes are affected and which HSA21 and non-HSA21 genes are associated with those processes are not fully understood. Furthermore, the extent to which human postmortem neuropathology is reflected in the mouse models (and vice versa) remains one of the key problems hampering further understanding of DS brain development and function.

Transcriptome profiling has provided insight into the pathophysiological mechanisms underlying neurodevelopmental brain disorders (Mitchell and Mirnics, 2012; State and Geschwind, 2015; Tebbenkamp et al., 2014). While several reports have investigated gene expression in postmortem human DS brains or derived pluripotent stem cells (Letourneau et al., 2014; Lockstone et al., 2007; Mao et al., 2003, 2005), these studies are limited by sparse genome coverage, numbers of samples or developmental time points, and potential variances between in vitro and in vivo gene regulation. We therefore set out to characterize the spatiotemporal dynamics of gene expression in the

CrossMark

DS and matched euploid brains and, subsequently, to decipher the biological processes affected over the course of prenatal and postnatal development.

Genome-wide transcriptional profiling was performed in different regions of male and female postmortem brains spanning from mid-fetal development to adulthood. This approach uncovered a highly dynamic disruption of the DS transcriptome across all chromosomes, with alterations in gene expression in different brain regions over time. Bioinformatic analysis revealed genes and gene networks for which expression was affected throughout the DS brain, revealing key molecular and cellular processes previously implicated in neurological dysfunction in DS as well as many that had not been well characterized in DS brains. Notably, we found transcriptome differences indicating that oligodendrocyte differentiation and myelination are altered in DS. We further identified cell-autonomous deficits in oligodendrocyte differentiation and the production of neocortical myelin, which were accompanied by slower action potential transmission between cerebral hemispheres. Altogether, the data illustrate disruption of distinct gene co-expression networks in DS, providing an extensive framework to identify, prioritize, and test gene candidates and biological processes underlying the neuropathophysiology of DS. To facilitate the usefulness and accessibility of the DS transcriptome, we also have generated an internet database (http://medicine.yale.edu/lab/sestan/resources/).

RESULTS

Genome-wide Spatiotemporal Alterations of Gene Expression in DS Brains

We used the Affymetrix exon array platform, which features comprehensive genome-wide coverage of the human transcriptome across entire transcripts and each individual exon, to characterize gene expression in different regions of DS brains over the course of development (see Experimental Procedures). Transcriptome profiling was performed using total RNA extracted from 11 regions, including multiple regions of the cerebral neocortex, the hippocampus (HIP), and the cerebellar cortex (CBC), using a standardized protocol from high-quality postmortem human brains of DS and clinically and anatomically unremarkable euploid controls (for details on tissue dissections, see the Supplemental Experimental Procedures, Figure S1, and Tables S1 and S2). We collected 58 paired tissue samples from 15 euploid control and 15 DS brains ranging in age from 14 post conception weeks (pcw) to 42 years old (Table S2), and we then allocated them into groups based on a previously described timeline that divides human brain development and adulthood into 15 periods (Kang et al., 2011).

Principal component analysis showed segregation between DS and control samples; however, brain regions and age (developmental periods) contributed more to the global differences in gene expression than disease status (Figure S2), indicating that gene expression in the human brain has a high degree of spatial variability (Table S2). We chose dorso-lateral pre-frontal cortex (DFC) and CBC for our analyses, because both regions have been implicated in DS neuropathology (Hartley et al., 2015; Haydar and Reeves, 2012; Letourneau et al., 2014; Lott, 2012) and exhibit diverse transcriptional profiles over the course

of development (Kang et al., 2011; Tebbenkamp et al., 2014). Of 17,557 mRNA genes profiled, 842 (4.8%) and 571 (3.25%) genes in DFC and CBC, respectively, were defined as significantly differentially expressed (DEX) between paired DS and euploid samples across all periods (Table S3) (false discovery rate [FDR] = 0.1; see the Supplemental Experimental Procedures). As expected, the percentage of DEX genes on HSA21 was higher than other chromosomes (Figures 1A and S3). While 19.5% (DFC) and 13.9% (CBC) of the genes localized on HSA21 were DEX genes, a median of 4.4% (DFC) and 3.0% (CBC) DEX genes were found on other chromosomes in DS compared to their matched control. However, the majority of DEX genes were non-HSA21 genes (1,337 genes versus 76 genes on HSA21) (Figure 1B). We also found that, while all HSA21 DEX genes were upregulated in DS samples, only 47.7% (DFC) and 45.2% (CBC) of non-HSA21 DEX genes were upregulated. Conversely, 52.3% (DFC) and 54.8% (CBC) of non-HSA21 genes were downregulated (Figure 1C), indicating that the triplication of HSA21 leads to both positive and negative regulation of genes on other chromosomes (Figure S4). This directionality of HSA21 gene expression profiles suggests that upregulation of genes on HSA21, some of which function as *trans* factors, is followed by up- and downregulation of genes distributed throughout the genome. Strikingly, we found that gene expression across all chromosome locations was altered even from 14 pcw, indicating early and widespread changes to the DS transcriptome.

A combination of sliding window, paired t test, and permutation tests was used to investigate temporal dynamics in transcriptional differences between DS and control brains (see the Supplemental Experimental Procedures). This analysis revealed that the number of DEX genes in DFC increased in an age-dependent manner, with significantly more DEX genes emerging over postnatal development and adulthood (periods 8–14) (Figure 1D; Table S4). A completely different temporal picture emerged in the CBC, where the number of DEX genes remained constant over development and adulthood (Figure 1E; Table S4). This dichotomy between the DFC and CBC temporal gene expression profiles extended throughout the genome, with more variability across all chromosomes over developmental time in DFC samples (Figure S3). Gene ontology enrichment analysis indicated potential dysregulated biological categories, including transmission of nerve impulse (Benjamini-Hochberg-adjusted [BHA] $p = 2.9 \times 10^{-8}$), synaptic transmission (BHA $p = 1.4 \times 10^{-5}$), cell morphogenesis (BHA $p = 1.4 \times 10^{-5}$), cell-cell signaling (BHA $p = 6.7 \times 10^{-5}$), and axon ensheathment (BHA $p = 4.8 \times 10^{-2}$) (Table S5).

Together, these studies demonstrate that many genes throughout the genome are altered in DS, confirming and extending previous findings that non-HSA21 genes may contribute significantly to trisomy 21 phenotypes (Letourneau et al., 2014; Lockstone et al., 2007). Most importantly, our results clearly show that many of these DEX genes display dynamic temporal and spatial differences in expression, and they highlight specific biological processes potentially disrupted in the developing DS brain.

Co-dysregulation of Genes Associated with Oligodendrocyte Differentiation and Myelination in DS

To integrate the expression differences observed between DS and matched control samples from all 58 paired samples and
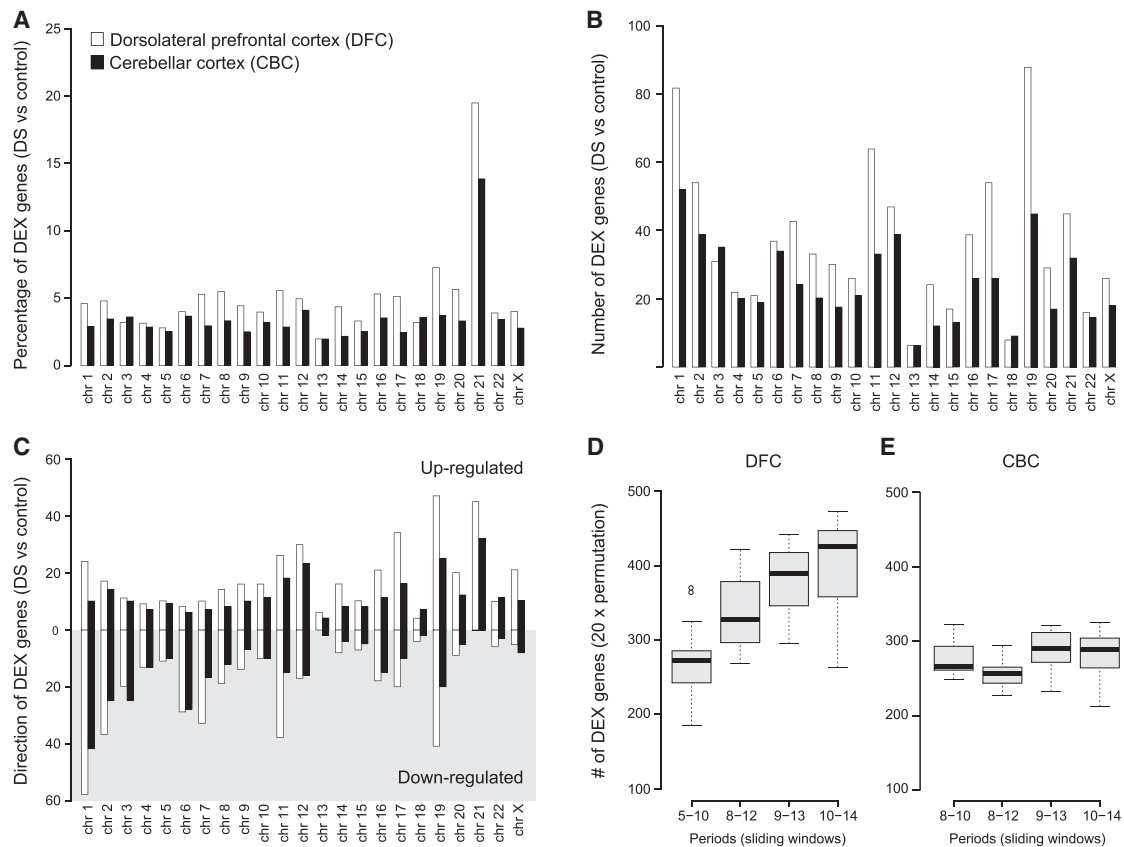
Figure 1. Genes Dysregulated in DS Brains Are Globally Distributed and Developmentally Dynamic

(A) The percentages of differentially expressed (DEX) genes on each chromosome are shown, indicating global disruptions in gene expression.

(B) The numbers of genes on each chromosome that are DEX in Down syndrome (DS). Note that the majority of DEX genes are not located on HSA21.

(C) The numbers of upregulated (white shading) and downregulated (gray shading) DEX genes per chromosome are shown.

(D and E) A permutation analysis of DEX genes in the dorsal frontal cortex (DFC) (D) and cerebellar cortex (CBC) (E) across four sliding windows corresponding to periods from mid-fetal development to adulthood. Periods of human brain development and adulthood are defined as previously described (Kang et al., 2011). Note that the number of DEX genes rises over development for DFC, but not CBC. No CBC samples were available for periods 5–7.

each brain region into a systems-level context, we performed weighted-gene co-expression network analysis (WGCNA) (Zhang and Horvath, 2005) and identified modules of co-expressed genes. We defined 60 gene modules exhibiting altered expression during DS brain development in the CBC, HIP, and multiple neocortical regions (Tables S6 and S7). We then carried out gene ontology enrichment analysis of each module to gain insight into the biological significance of these clusters of co-expressed genes (Table S6). This analysis confirmed a number of cellular and molecular processes previously found to be altered in DS or mouse model brains, including cell morphogenesis (Module [M] 24; Figure S5A), RNA processing (M31), gene transcription (M52), immune responses (M54; Figure S5B), neuronal differentiation (M4 and M45; Figures S6A and S6D), synaptic transmission and regulation (M10 and M34; Figures S6B and S6C), and electron transport (M14) (Table S6; Bahn et al., 2002; Lockstone et al., 2007; Sahún et al., 2014; Yoshida et al., 2013; Zampieri et al., 2014).

WGCNA also identified co-expression modules enriched for genes associated with biological processes previously not well

characterized in DS. Notably, a module of co-expressed genes, number 43 (M43), was enriched for gene ontology categories related to regulation of action potential (BHA p = 1.7 × 10−2) and axon ensheathment (BHA p = 3.7 × 10−2), and it was markedly downregulated throughout the DS neocortex and in the HIP over development (Figures 2A and 2B; Table S6). Differences in this module accelerated over the course of DS neocortical development (Figures 2A and 2B), coinciding with the onset and progression of myelination. Note that the absence of an M43 expression phenotype in the CBC of DS brains (Figures 2A and 2B) is likely because the most numerous cells in CBC, granule cells, have unmyelinated axons.

To further characterize M43 genes, we investigated whether they were associated with the developmental program of specific neural cell types (i.e., astrocytes, endothelial cells, microglia, neurons, oligodendrocyte progenitor cells, newly formed oligodendrocytes, or myelinating oligodendrocytes). We queried whether M43 genes that were highly expressed (fragments per kilobase per million mapped reads [FPKM] > 20) in different populations of neural cell types purified from mouse cerebral cortex
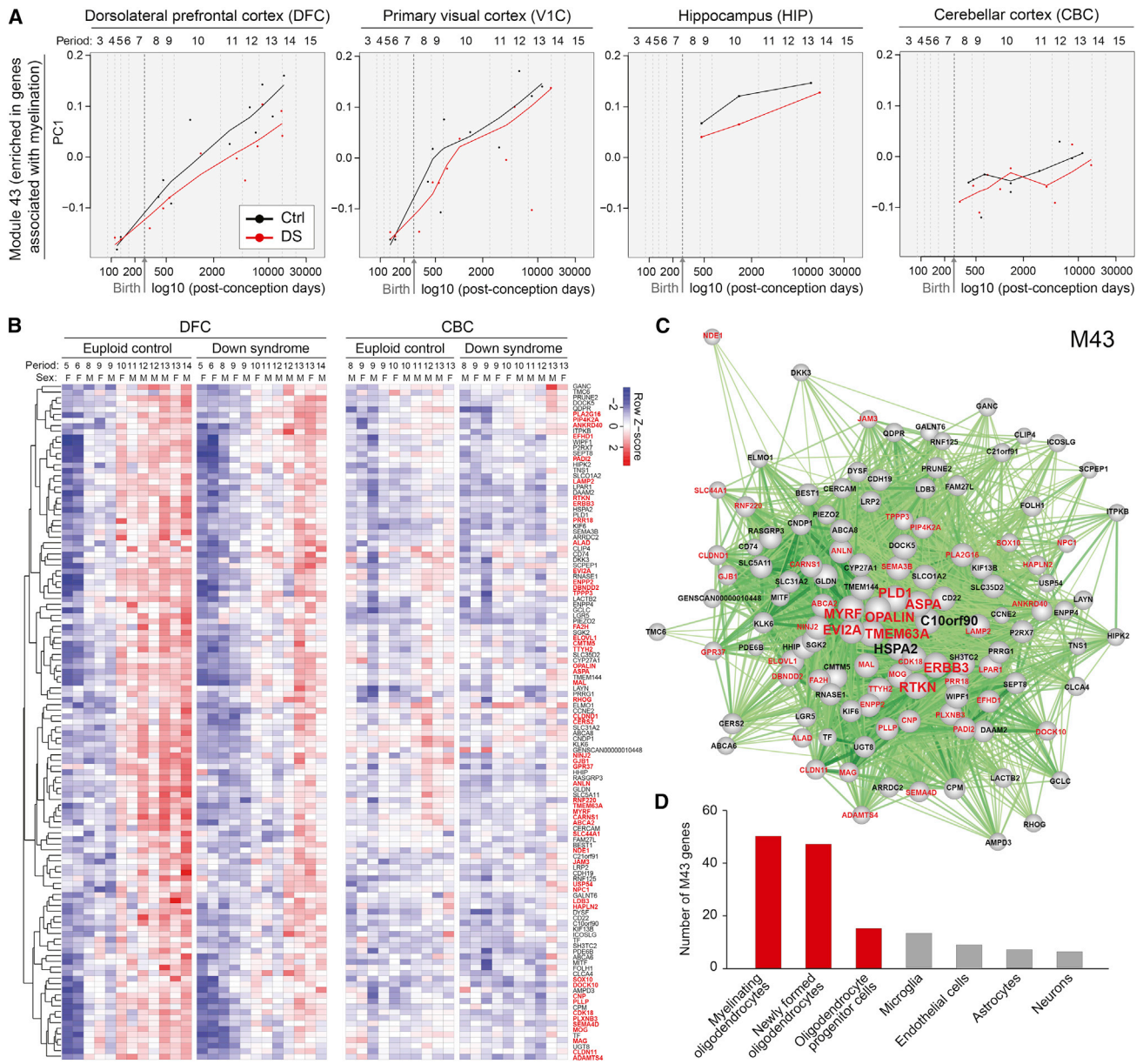
Figure 2. A Co-expression Module Enriched in Genes Associated with Oligodendrocyte Development and Myelination Is Decreased over Development in DS

(A) Gene network analysis identifies distinct modules of co-expressed genes dysregulated in DS, including module (M)43 that is significantly enriched in genes associated with oligodendrocyte development and myelination. Plots show relative expression of the PC1 of M43 over development in the DFC, primary visual cortex (V1C), hippocampus (HIP), and CBC, indicating higher expression in euploid control versus DS brain that increases in degree over development.

(B) A heatmap showing the expression of M43 genes in DFC (left) and CBC (right), which confirms and details the gene expression trajectories shown in (A). Note that a high proportion of mouse homologs of the M43 genes are expressed in mouse oligodendrocyte lineage cells (gene symbols are highlighted in red).

(C) A network plot of M43 genes and their intramodular connections (cutoff, Pearson correlation > 0.7). Eight of the ten hub genes (the top ten genes with highest intramodular connectivity; *TMEM63A, MYRF, PLD1, RTKN, ASPA, OPALIN, ERBB3,* and *EVI2A*) are primarily expressed by mature oligodendrocytes and tightly correlated with other oligodendrocyte-associated M43 genes. Oligodendrocyte-enriched genes are shown in red. Note their central position in the network, suggesting high intramodular connectivity.

(D) The number of mouse homologs of M43 genes that are highly expressed in major cell types from mouse cerebral cortex. The majority of the M43 genes are highly expressed specifically in oligodendrocytes. Red bars denote the oligodendrocyte lineage; gray bars denote other cell lineages.

(Zhang et al., 2014; see the Supplemental Experimental Procedures). We found that, of the 121 mouse homologs of genes in M43, 67 met this cutoff for high expression (FPKM > 20) and

82.1% (55/67) of this subset were found to be highly expressed by oligodendrocyte lineage cells (gene names labeled in red in Figures 2B–2D). Importantly, eight of the top ten genes with

highest intramodular connectivity (hub genes) in M43 were primarily expressed by mature oligodendrocytes and tightly correlated with other oligodendrocyte-associated M43 genes (Figure 2C).

To ensure that DEX genes were not detected due to variability in tissue dissections, we analyzed genes highly enriched in astrocytes, neurons, and oligodendrocytes (Zhang et al., 2014; see the Supplemental Experimental Procedures). We found that intra-individual gene expression for these three cell types was highly correlated in all samples (see Table S8). We further found by pairwise analysis that gene expression levels for markers of all three cell types were highly correlated for the same brain regions in all control ($r > 0.94$) or DS individuals ($r > 0.95$), indicating uniform tissue collection procedures. However, in agreement with our DEX analysis, expression of oligodendrocyte-specific genes was less correlated and significantly different between DS and control DFC ($r = 0.89$, $p = 0.018$ Wilcoxon signed-rank test; Table S8).

We analyzed individual expression trajectories of several genes within the M43 module known to be expressed in oligodendrocytes and involved in myelination. Lower levels of gene expression spanning from birth to adulthood for myelin-associated glycoprotein (MAG; Figure 3A) and from mid-fetal development to early childhood for myelin basic protein (MBP; Figure 3B) were observed. To validate the MAG and MBP exon array data, we assayed the expression of these white matter-associated genes and their gene products in the same neocortical samples using digital droplet PCR (ddPCR) (Figure 3C) and immunoblotting (Figures 3D–3F). Together, both DEX and WGCNA analyses provide evidence for alterations in neocortical oligodendrocyte differentiation and myelination in developing DS brains at transcript and protein levels.

Given these substantial changes in oligodendrocyte lineage genes and proteins, we sought to confirm previous reports of reduced myelination in the DS forebrain. We imaged tissue sections of the DFC from five pairs of human DS and matched control specimens, ranging in age from 1 to 70 years old, using the spectral confocal reflectance microscopy (SCoRe) technique (Schain et al., 2014). Consistent with previous reports, we found that the overall density of myelinated fibers is reduced in DS brain across all ages (Figures S6A and S6B). In addition, we found that myelinated axons in control brains form a grid-like lattice that resembles a rectilinear grid, as described previously (Ang et al., 2003; Wedeen et al., 2012; Figure S6C). However, DS brains did not exhibit evidence of grid-like myelinated fiber orientations, suggesting reduced complexity of fiber pathways in the trisomic human brain.

White Matter Abnormalities in a Trisomic Mouse Model of DS

To determine whether the protein- and cellular-level consequences of altered oligodendrocyte/myelination-associated gene expression in DS also are reflected in mouse models, we examined oligodendrocyte lineage progression, myelination, and neuronal conductivity over development in the Ts65Dn mouse brain. This commonly used DS model is trisomic for ~100 orthologs of the 364 genes on HSA21 and displays many DS-specific phenotypes, including delays in

brain development and cognitive defects (Rueda et al., 2012). However, changes in white matter have not been previously described in the Ts65Dn mouse brain. By immunoblotting of neocortex tissue samples (n = 10) (Figure 3G) and immunostaining of the anterior cingulate cortex and underlying corpus callosum (n = 9) (Figure 3H), we found a reduction of MAG (Figures 3G and 3H) and MBP (Figures 3I and 3J) protein levels and immunostaining intensity in postnatal day (P)30 Ts65Dn mice. Reduced immunostaining intensity for 2′,3′-cyclic nucleotide 3′ phosphodiesterase (CNP), an oligodendrocyte- and myelin-associated protein, also was observed in the P60 neocortex in Ts65Dn brains (Figure S7). Importantly, these cellular and biochemical changes are first detected during the period of myelin development and refinement and are maintained at later ages (e.g., P60).

Myelin, Axon, and Action Potential Conduction Deficits in Trisomic White Matter

Alterations in white matter-associated proteins measured within the trisomic human and mouse brains indicate possible changes in the amount or allocation of myelin. We tested this hypothesis with ultrastructural and immunofluorescent studies in Ts65Dn and euploid mice at P60. Electron microscopy revealed that axon profiles in the Ts65Dn corpus callosum are on average larger than in controls (Figures 4A and 4B), and there was a trend for fewer myelinated axons in the body of the Ts65Dn corpus callosum (p = 0.1, n = 6; Figure 4C). Furthermore, when myelinated axons were binned by axon area, we found a significant decrease in the number of small-bore myelinated axons (0–0.5 μm^2, p = 0.046; Figure 4D). We also found that myelinated axons in Ts65Dn brains have significantly thinner myelin sheaths (g ratio, p < 0.011; Figures 4E and 4F). Axons were then binned by size to determine whether a correlation exists between axon diameter and myelin sheath thickness. Specifically, small-bore myelinated Ts65Dn axons within 0–0.5 and 0.5–1 μm^2 have thinner myelin sheaths than corresponding controls (p = 0.084 and p = 0.076, respectively; Figure 4G). Altogether, these results indicate a decrease in the percentage of small-bore myelinated axons and myelin sheath thickness in Ts65Dn white matter.

Deficits in myelination and oligodendrocyte maturation also can lead to impaired formation of the nodes of Ranvier (Kaplan et al., 2001; Rasband et al., 1999; Tanaka et al., 2009). Therefore, we immunostained coronal brain sections from Ts65Dn and controls for NF186 (an NFASC isoform) and CNTNAP1 (Thaxton et al., 2010), which mark nodal regions. Quantification of nodal protein profiles in the Ts65Dn brain at P60 revealed a striking decrease in the number of nodes of Ranvier in the corpus callosum, and we found similar decreases in the external capsule (Figures 5A–5C; p < 0.005). Ultrastructural analysis confirmed this result, revealing a trend for fewer paranode cross-sections in Ts65Dn (Figures 5D and 5E; p = 0.059). To determine if these findings implicate changes in node formation as a novel human DS brain phenotype, we evaluated expression levels of both NFASC and CNTNAP1 in the exon array dataset. These genes were significantly downregulated from birth to adulthood (Figures 5F and 5G), and subsequent ddPCR analysis confirmed these differences in the DS brain samples (Figure 5H).
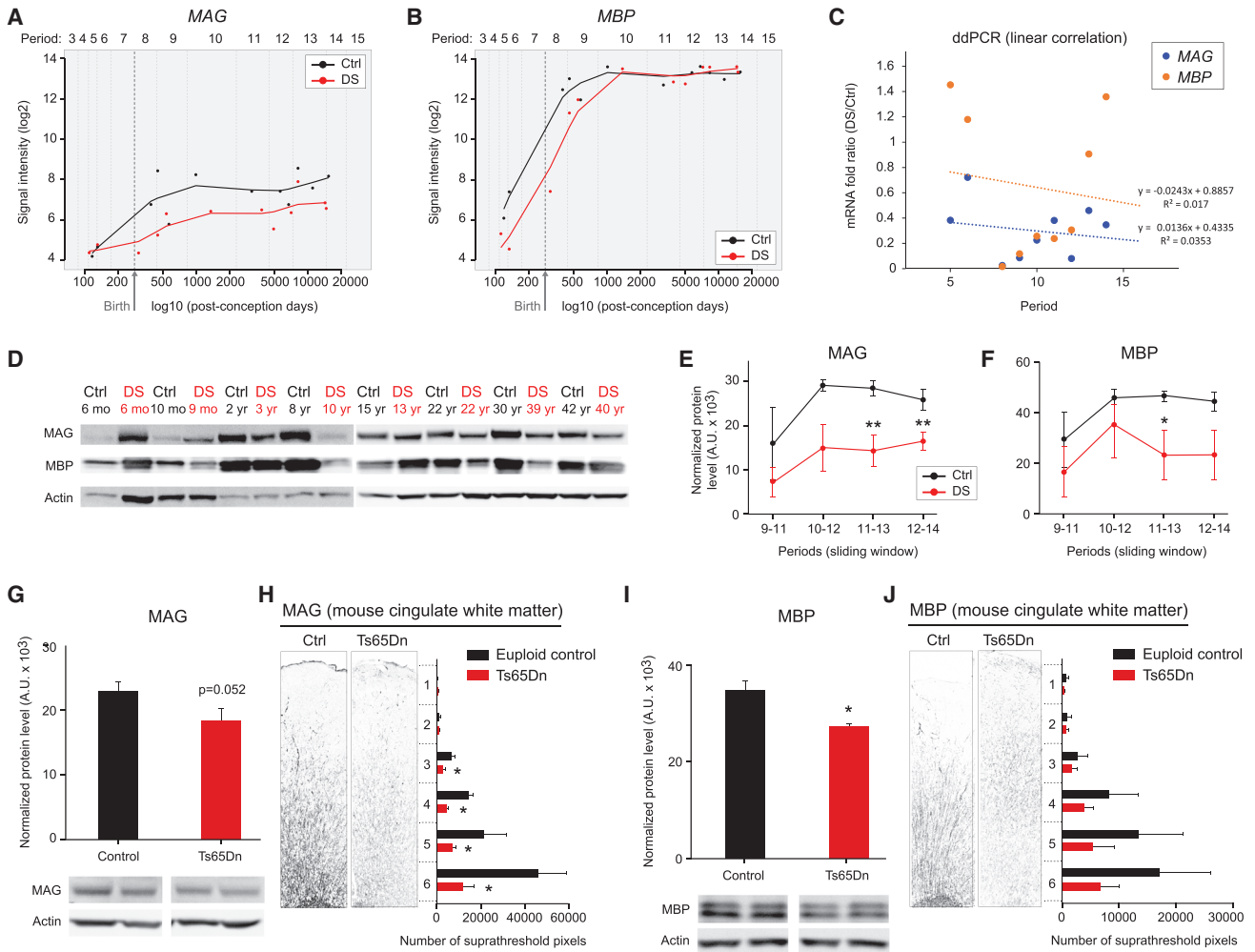
Figure 3. Expression of the Essential Myelin Components MAG and MBP Is Diminished in Developing DS and the Ts65Dn Mouse Brains

(A) Log2 values of the array signal intensity in human euploid control (Ctrl) and DS DFC show that *MAG* expression is decreased from birth onward (periods 8–14) in DS. Periods 5–9, $p = 0.28$; periods 8–12, $p = 0.023$; periods 9–13, $p = 0.025$; periods 10–14, $p = 0.0024$; all periods, $p = 0.014$ (paired t test).

(B) Log2 values of the array signal intensity in human Ctrl and DS DFC show that *MBP* expression is decreased from mid-fetal development to early childhood (periods 5–9) in DS. Periods 5–9, $p = 0.078$ (one-tailed test, $p = 0.039$); periods 8–12, $p = 0.192$; periods 9–13, $p = 0.52$; periods 10–14, $p = 0.72$; all periods, $p = 0.10$ (paired t test).

(C) The ddPCR analysis of *MBP* and *MAG* expression in human Ctrl and DS DFC samples confirms decreased expression in developing DS brains.

(D) Representative western blots for MAG and MBP in human Ctrl and DS DFC over development are shown (DS samples in red type).

(E and F) Sliding-window analysis of MAG (E) and MBP (F) protein levels identify significant reductions in developing and adult DS brains. *$p \leq 0.03$ (paired t test).

(G and H) Western blotting of neocortex tissue samples (n = 10) (G) and immunostaining of the anterior cingulate cortex (n = 9) (H) in postnatal day (P)30 Ctrl and trisomic Ts65Dn mice identify a reduction of MAG protein expression in Ts65Dn brains. *$p \leq 0.05$ and **$p \leq 0.001$ (paired t test).

(I and J) Western blotting for MBP in the neocortex (n = 3 pairs) (I) and immunostaining for MBP in P30 cingulate cortex (J) of Ctrl and Ts65Dn mice show a trend toward reduced expression of MBP in the white matter of Ts65Dn mice (n = 3 pairs). *$p = 0.009$ (paired t test).

To determine the functional consequences of these white matter defects, we measured compound action potentials in the corpus callosum of P30–P55 Ts65Dn forebrain slices (Figure 6A). Our results revealed that action potential transmission is significantly slower in myelinated Ts65Dn axons (N1) compared to euploid controls (Figure 6B; $p = 0.04$, n = 10). In contrast, the conduction velocity in unmyelinated axons (N2) is similar between groups (Figure 6B; $p = 0.4$, n = 11). Examining the relationship between stimulus intensity and response magnitude (input-output curve) revealed that both types of axons in Ts65Dn are less excitable than those in euploid mice (Figures 6C and 6D; $p < 0.001$ for N1 and $p < 0.007$ for N2). However, the action potential refractory periods were not different between groups, indicating that sodium channel kinetics are less likely to be responsible for the shift in the input-output relationship (data not shown). These data, combined with our cellular and electron microscopy results, indicate that white matter abnormalities found in the trisomic human and Ts65Dn mouse brains contribute to structural and functional defects in neurotransmission.
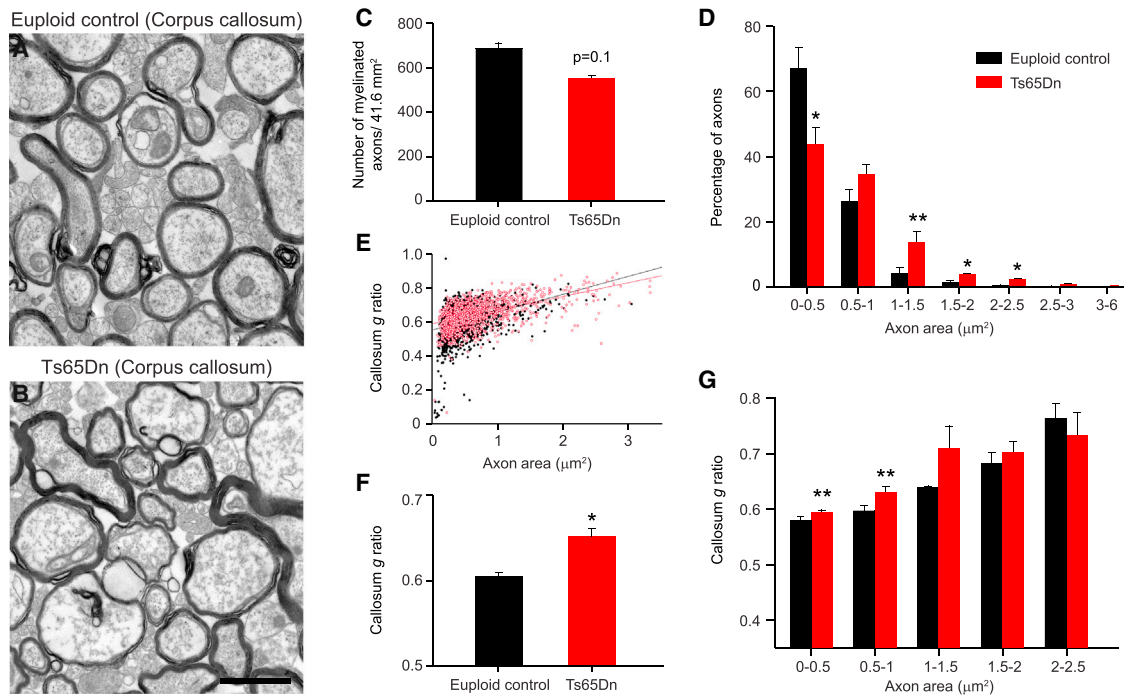
Figure 4. Diminished Myelin Sheath Thickness in the Ts65Dn Corpus Callosum

(A and B) Representative electron micrographs show axon cross sections in the P60 euploid control (A) and Ts65Dn (B) corpus callosum. Scale bar, 1 μm.

(C) Graph of the numbers of myelinated axons in euploid versus Ts65Dn reveals a trend toward a decrease in the number of myelinated axons in Ts65Dn mice.

(D) Histogram indicates a decrease in the proportion of small diameter axons and an increase in the proportion of large diameter axons (>1 μm) in Ts65Dn mice. *p $\leq$ 0.05 and **p = 0.058 (paired t test).

(E) Plot shows g ratios (y axis) and the corresponding diameter for all axons assessed. Black dots, euploid control; red dots, Ts65Dn.

(F) Bar graph shows there is a significant increase in the mean g ratio in Ts65Dn mice, indicating thinner myelin sheaths around Ts65Dn axons. *p = 0.011 (paired t test).

(G) Histogram indicates that the g ratios of small diameter, but not large diameter, axons are higher in Ts65Dn mice. **p $\leq$ 0.08 (paired t test [not significant]).

Alterations in Oligodendrocyte Lineage Progression in DS and Trisomic Mouse

To gain further insight into possible underlying mechanisms for myelin and white matter defects in DS, we examined the expression of genes associated with the development of human oligodendrocyte precursor cells and mature oligodendrocytes by generating sets of genes predicted to be selectively enriched in these cell types during human development. These gene sets were generated by overlapping lists of oligodendrocyte lineage candidate genes from previous mouse (Zhang et al., 2014) and human (Kang et al., 2011) studies (for details on the gene selection and analysis, see the Supplemental Experimental Procedures and Table S9). We then assessed if there was differential expression of the oligodendrocyte precursor and myelinating oligodendrocyte gene sets in DS versus control DFC. We observed that expression of putative human oligodendrocyte precursor cell-related genes gradually increases in DS compared to controls, persisting until periods 12–14 (Figure 7A). In contrast, putative human myelinating oligodendrocyte genes in the DFC are expressed at lower levels from birth into adulthood (Figure 7C). These data support and extend our DEX and WGCNA analyses (Figure 2; Tables S5 and S6), suggesting an overall and long-lasting impairment of oligodendrocyte maturation in DS, which is detectable after birth in the neocortex.

To characterize these changes at the gene network level, we determined the overlap between WGCNA modules and sets of genes that we predicted to be selectively enriched in oligodendrocyte precursor cells or myelinating oligodendrocytes (Table S9). We found that human oligodendrocyte precursor cell genes were significantly enriched in modules M9, M36, M43, and M47 (Figure 7B); exon array trajectories for the two most significantly enriched modules (i.e., M9 and M47) indicated elevated expression in DS brain samples over the course of development (Figure 7E). Conversely, human mature oligodendrocyte genes were found to be significantly enriched primarily in two modules, M8 and M43, and their trajectories indicated decreased expression in DS brains during development (Figures 7D and 7F). Thus, the relevant WGCNA modules exhibit similar trajectories when compared with the expression changes of individual oligodendrocyte lineage genes, demonstrating that these cell-type-specific defects in oligodendroglial development are associated with complex gene network disturbances in the DS brain. Altogether, these data indicate that aberrations in the process of oligodendrocyte maturation to the myelinating stage may underlie the white matter abnormalities in DS.

To test whether differences observed through our transcriptomic analyses identify changes in the oligodendrocyte lineage at the cellular level, we performed a developmental study of
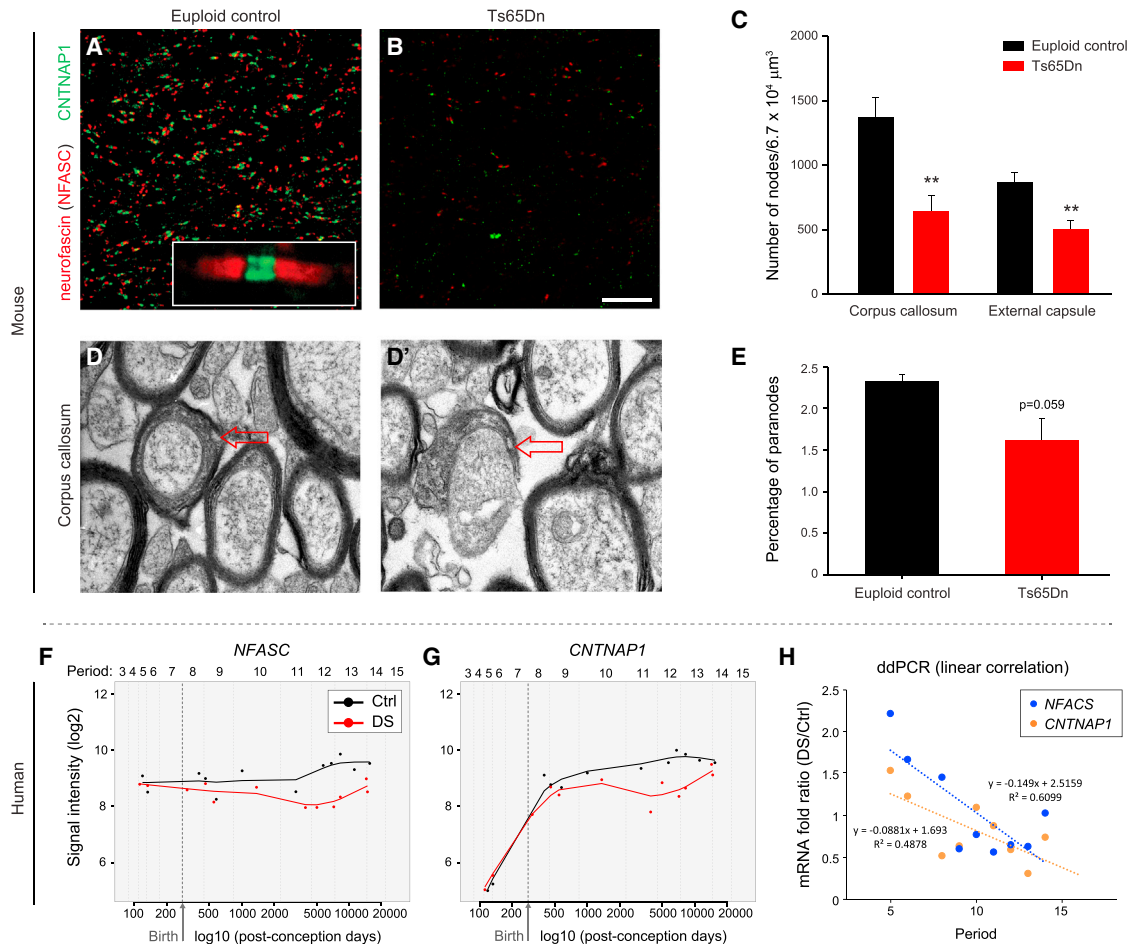
Figure 5. Impaired Formation of Nodes of Ranvier in Ts65Dn Mice

(A) Representative image shows nodes of Ranvier in P60 euploid control (Ctrl) corpus callosum identified by immunofluorescent labeling for the paranodal protein NFASC (red) and the internodal protein CNTNAP1 (green), which mark the node of Ranvier.

(B) Representative image shows immunostaining for NFASC (red) and CNTNAP1 (green), indicating there are fewer nodes of Ranvier in Ts65Dn mice.

(C) Bar graph demonstrates reduced density of nodes of Ranvier in corpus callosum and external capsule in P60 Ts65Dn brain (n = 3 pairs). **p $\leq$ 0.002 (paired t test).

(D and D') Electron micrographs show representative images of paranodes (arrows).

(E) Quantification of paranodes reveals that they are reduced in P60 Ts65Dn corpus callosum (n = 3 each).

(F) Log2 values of the array signal intensity in human euploid Ctrl and DS DFC show that *NFASC* expression is decreased from birth onward (periods 8–14) in DS. Periods 5–9, p = 0.23; periods 8–12, p = 0.016; periods 9–13, p = 0.0092; periods 10–14, p = 0.0022; all periods, p = 0.0028 (paired t test).

(G) Log2 values of the array signal intensity for DFC expression of *CNTNAP1* show that its expression is decreased from birth onward (periods 8–14) in DS. Periods 5–9, p = 0.41; periods 8–12, p = 0.018; periods 9–13, p = 0.017; periods 10–14, p = 0.011; all periods, p = 0.012 (paired t test).

(H) The ddPCR analysis of human DFC samples confirms decreased expression of *NFASC* and *CNTNAP1* from childhood onward in DS.

the Ts65Dn corpus callosum from P7 to P60 (Figures 7G–7I). We first immunostained for OLIG2 to mark the oligodendrocyte lineage and CC1 or NG2 to identify myelinating oligodendrocytes or oligodendrocyte precursor cells, respectively. At P7, around the onset of myelination, we found equivalent numbers of OLIG2+, CC1+, and NG2+ cells in Ts65Dn and control brain white matter. However, during the ensuing periods of active myelination and thereafter (after P7 and up to P60), there were fewer OLIG2+ cells in the Ts65Dn white matter compared to controls, reaching significance at P60; this decline in numbers was not due to higher than normal apoptotic rates (data not shown). More importantly, compared to controls and as predicted by the human transcriptome study, there was a higher percentage of OLIG2+/NG2+

oligodendrocyte precursor cells and a decreased percentage of OLIG2+/CC1+ oligodendrocytes in Ts65Dn white matter from P15 on. These results demonstrate that changes in the ratio of oligodendrocyte precursor cells to mature oligodendrocytes develop during the period of active myelination.

Finally, we sought to determine if there were cell-autonomous effects of Ts65Dn chromosomal triplication on oligodendrocyte development by carrying out proliferation and maturation assays of purified oligodendrocyte progenitor cells isolated by immunopanning with an antibody against alpha-type platelet-derived growth factor receptor (PDGRA or PDGFRα) (Figure 8). Effects on oligodendrocyte progenitor cell proliferation were assayed by plating euploid control and Ts65Dn oligodendrocyte
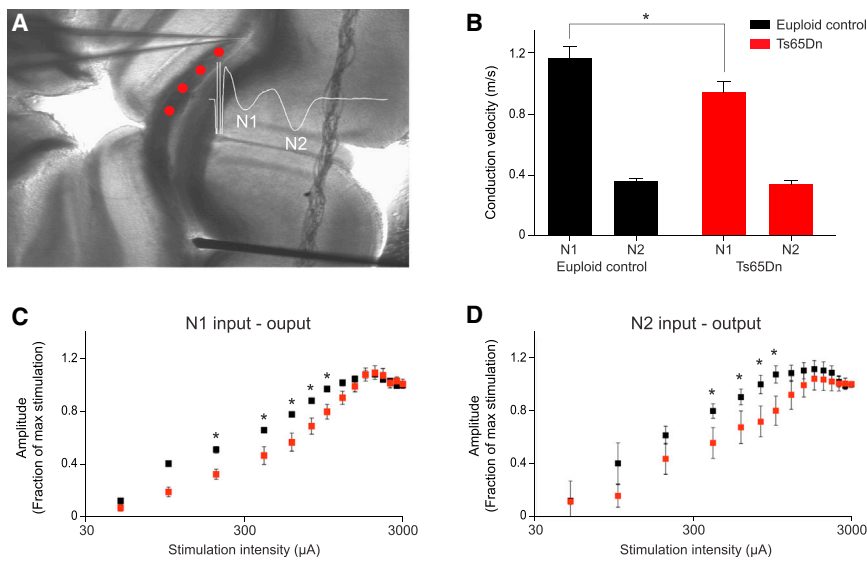
Figure 6. Slower Axonal Conduction in Ts65Dn Corpus Callosum

(A) Experimental setup depicting the stimulating electrode (bottom) and recording electrode (top) within P30 corpus callosum of a coronal section. Compound action potentials (CAPs) evoked by stimulation were recorded at multiple sites (red dots) to compute conduction velocity. Inset shows a representative example of an evoked CAP depicting the components arising from myelinated fibers (N1) and unmyelinated fibers (N2).

(B) Bar plot showing that conduction velocities for myelinated fibers (N1), but not unmyelinated fibers (N2), were significantly slower in Ts65Dn corpus callosum. $*p = 0.04$ ($n = 10$ for N1 and $n = 11$ for N2).

(C) The input-output relationship for myelinated fibers is right-shifted in Ts65Dn corpus callosum, suggesting that this fiber type is less excitable. $*p < 0.001$ for N1 (euploid $n = 5$ and Ts65Dn $n = 4$).

(D) The input-output relationship for unmyelinated fibers is right-shifted in Ts65Dn corpus callosum, suggesting that this fiber type is less excitable. $*p \leq 0.007$ for N2 (euploid $n = 5$ and Ts65Dn $n = 4$).

progenitor cells at the same density in proliferative conditions for 48 hr. We found no difference in the number of OLIG2/PDGFRA oligodendrocyte progenitor cells in cultures derived from euploid and Ts65Dn mice (Figures 8A, 8B, and 8E).

To test for effects of trisomy on oligodendrocyte maturation, oligodendrocyte progenitor cells were differentiated for 72 hr. The cells were stained for MBP and OLIG2 (Figures 8C and 8D). MBP+/OLIG2+ cells were considered mature, whereas MBP− cells were considered immature. We found that the total number of OLIG2 cells was diminished in Ts65Dn cultures after 72 hr, suggesting that Ts65Dn cell viability is reduced in these conditions (Figures 8C, 8D, 8F, and 8G). In addition, the percentage of OLIG2+/MBP+ cells was significantly diminished. To further assess this possibility, we characterized the morphology of MBP+ cells in each culture. We found that a greater proportion of Ts65Dn-derived MBP+ cells displayed a simple morphology compared to euploid cells (Figure 8H). Taken together, these cell culture experiments indicate that Ts65Dn oligodendrocytes exhibit cell-autonomous impairments in oligodendrocyte maturation and viability, but not proliferation.

DISCUSSION

In this study, we provide the most comprehensive developmental analysis of gene expression in postmortem human DS brains and their respective age-matched controls to date, and, thereby, we establish a novel framework for the study of neural development in DS. This effort has elucidated three key aspects of gene expression differences between DS and euploid control brains. First, dysregulated genes are found throughout the genome and are not present solely on HSA21. Second, many of the dysregulated genes exhibit highly specific temporal and regional expression profiles. Third, these dysregulated genes form distinct co-expression networks associated with distinct biological categories, providing novel and unbiased insight into the multiple biological processes affected in developing and adult DS brains. Viewing DS brain development through this

new lens, we have uncovered novel and robust abnormalities in the expression of genes associated with oligodendrocyte development and myelination.

Our assessment of Ts65Dn mice provided strong confirmation of the human oligodendrocyte and white matter defects, and it identified cell-autonomous impairments in oligodendrocyte maturation and viability, but not proliferation, as the underlying mechanism. These close similarities allowed us to further assess the cellular and functional consequences of these abnormalities, identifying changes in action potential conductance velocity in the forebrain white matter. These results elucidate a continuum of myelination-associated defects at the molecular, structural, and functional levels that likely contribute to developmental delays and life-long intellectual disability in DS.

The chromosomal location of the dysregulated genes identified in our study indicates a scattered, widespread distribution throughout the genome. It has been shown recently by Letourneau et al. (2014), in fibroblasts from monozygotic twins discordant for trisomy 21, that the DS-altered gene expression follows a consistent pattern with increased and decreased gene expression levels alternating across large chromosomal segments, which they named gene expression dysregulation domains (GEDDs). These GEDDs were not observable when comparing grouped samples due to gene expression differences between individuals, and this is consistent with our results (Figure S4). It therefore remains unclear whether and how these individual-specific GEDDs underlie cardinal features of DS brain development and function. Nevertheless, in the present study, we show that dysregulated genes, despite being present throughout the genome, are organized into multiple gene networks that are robust enough to be measured across multiple samples of unrelated individuals. Most importantly, by elucidating the in vivo impact of the white matter-associated gene modules as an example, we show that these systems-level changes impact cellular development and play a functional role in brain maturation.

We uncovered substantial differences between brain regions in the number and identities of altered genes, and we demonstrated
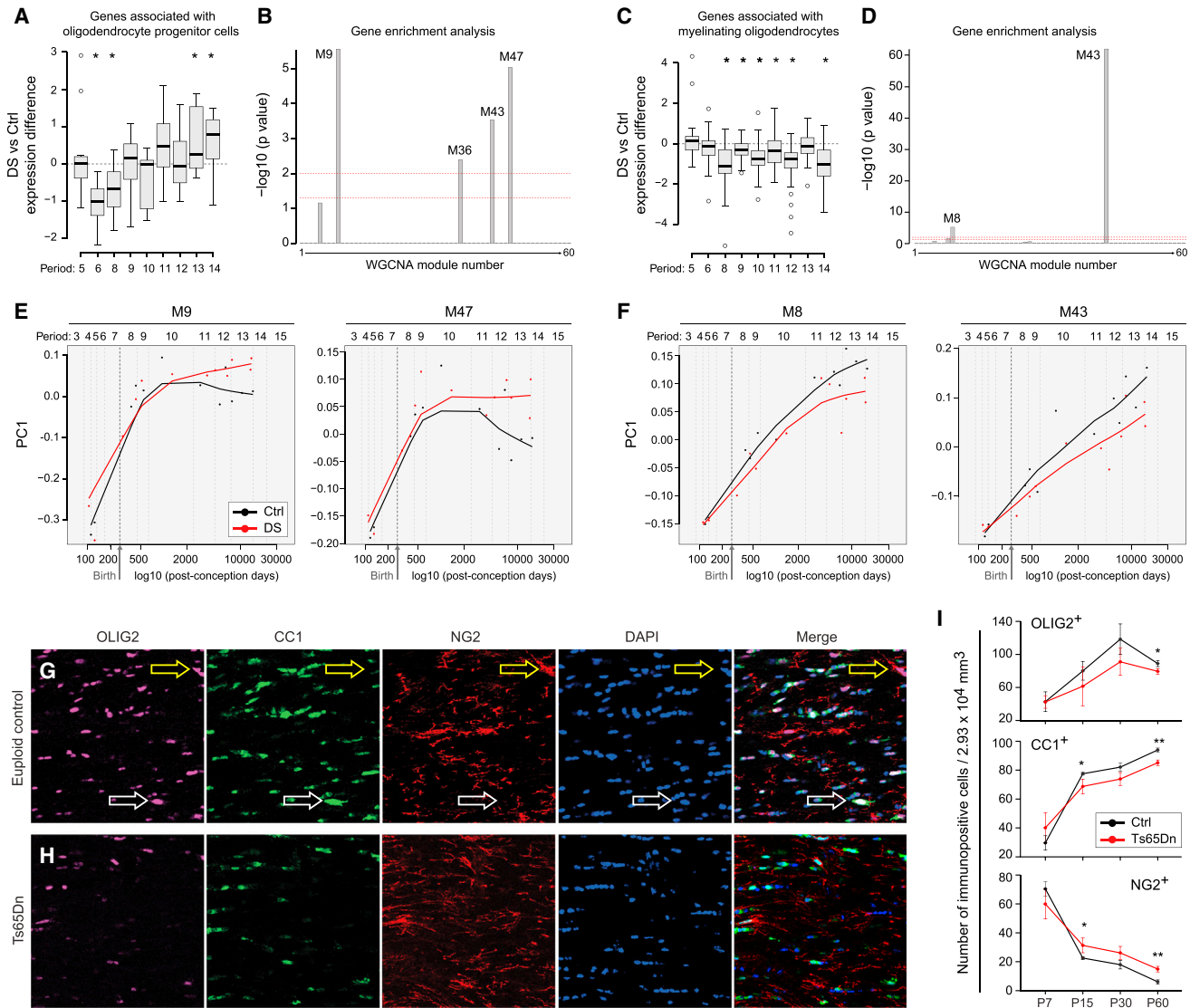
Figure 7. Oligodendrocyte Maturation Is Impaired in DS

(A) Developmental changes in genes associated with oligodendrocyte progenitor cells, expressed as a ratio of DS versus Ctrl, are shown. *$p \leq 0.05$ (paired t test).

(B) The $-\log10$ p values of expression of oligodendrocyte progenitor cell-enriched genes in weighted-gene co-expression network modules reveal significant enrichment in the M9, M36, M43, and M47 modules (y axis, $-\log10$ [p value]). Lower dashed line corresponds to $p = 0.05$; upper dashed line corresponds to $p = 0.01$.

(C) Developmental changes in genes associated with myelinating oligodendrocytes, expressed as a ratio of DS versus Ctrl, are shown. *$p \leq 0.05$ (paired t test).

(D) The $-\log10$ p values of enrichment analysis for expression of mature oligodendrocyte-enriched genes in gene network co-expression modules demonstrate significant enrichment in modules M8 and M43 (y axis, $-\log10$ [p value]). Lower dashed line corresponds to $p = 0.05$; upper dashed line corresponds to $p = 0.01$.

(E) PC1 plots of the co-expression modules enriched in oligodendrocyte progenitor cell-specific genes (M9 and M47) demonstrate that they are increased in DS and that the differences between Ctrl and DS samples increase over postnatal development.

(F) PC1 plots of the co-expression modules enriched in specific myelinating oligodendrocyte-specific genes (M8 and M43) demonstrate that they are decreased in DS and that the differences between Ctrl and DS samples increase over postnatal development.

(G) Representative immunofluorescent stains of P60 Ctrl corpus callosum for OLIG2 (purple), CC1 (green), NG2 (red), and nuclei (blue). Yellow arrows point to NG2-labeled oligodendrocyte progenitor cells and white arrows point to CC1-labeled mature oligodendrocytes.

(H) Representative immunofluorescent stains of P60 Ts65Dn corpus callosum for OLIG2 (purple), CC1 (green), NG2 (red), and nuclei (blue). Fewer CC1-labeled mature oligodendrocytes are apparent.

(I) The numbers of OLIG2 immuno-positive cells in the corpus callosum were counted in image volumes from P7 to P60 (n = 4 pairs at each age). There was a general trend of fewer OLIG2+ cells in the Ts65Dn white matter, which becomes significant at P60. In addition, as a proportion of the total OLIG2+ population, the percentage of NG2+ oligodendrocyte progenitor cells is higher in Ts65Dn corpus callosum from P15 to P60. In contrast, the percentage of mature CC1+ oligodendrocytes is reduced in Ts65Dn from P15 to P60. *$p \leq 0.05$ and **$p \leq 0.005$.
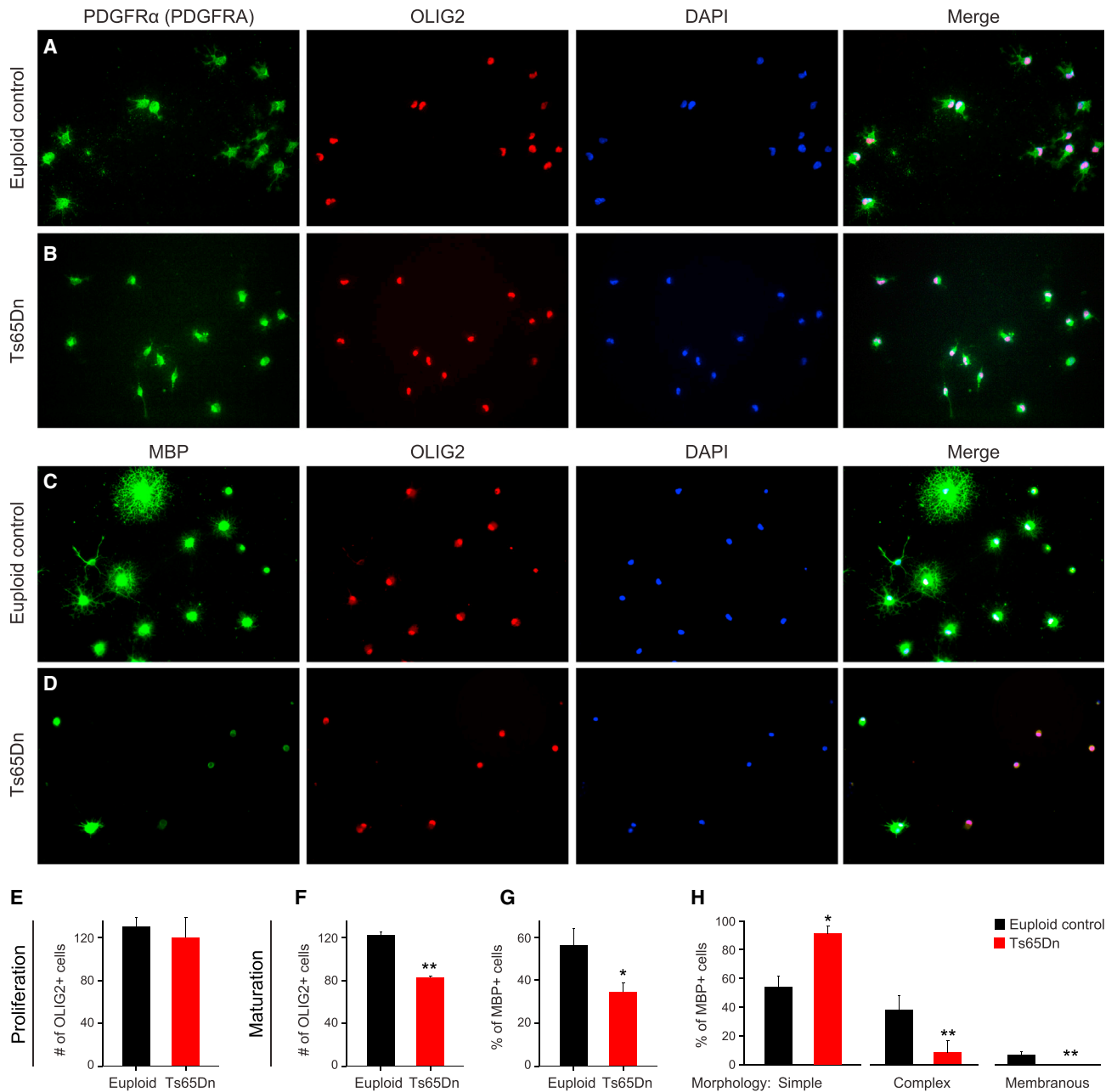
Figure 8. Impaired Maturation and Viability of Immunopurified Oligodendrocyte Progenitor Cells In Vitro

(A) Representative micrographs show immunostaining for oligodendrocyte progenitor cells isolated from P7 euploid cortex and proliferated for 48 hr. PDGFRA, green; OLIG2, red; nuclei, blue.

(B) Representative micrographs show immunostaining for oligodendrocyte progenitor cells isolated from P7 Ts65Dn and proliferated for 48 hr. PDGFRA, green; OLIG2, red; nuclei, blue.

(C) Representative micrographs show immunostaining for oligodendrocyte progenitor cells isolated from P7 euploid cortex and cultured in pro-maturation conditions for 72 hr. MBP, green; OLIG2, red; nuclei, blue.

(D) Representative micrographs show immunostaining for oligodendrocyte progenitor cells isolated from P7 Ts65Dn cortex and cultured in pro-maturation conditions for 72 hr. MBP, green; OLIG2, red; nuclei, blue.

(E) Graph indicates there were no differences between euploid control and Ts65Dn in the number of OLIG2+ cells observed after 48 hr in proliferative conditions.

(F) Graph indicates the number of OLIG2+ cells was reduced by ∼30% after 72 hr in pro-maturation conditions.

(G) Graph indicates the percentage of OLIG2+ cells co-expressing MBP was reduced by ∼40% after 72 hr in pro-maturation conditions.

(H) Graph indicating a greater percentage of MBP+ cells from Ts65Dn mice cultured in pro-maturation conditions exhibited a simple morphology (less than six processes) than MBP+ euploid cells, which tended to have a more complex (six or more processes) or membranous morphology. *p ≤ 0.05 and **p ≤ 0.01 (unpaired Student's t test).

temporal changes in these region-specific expression profiles. When considered together, these data indicate that the neurobiology of DS cannot be characterized by static lists of dysregulated genes or gene networks. Instead, the spatiotemporal nature of the disturbance plays a large role over the course of development and adulthood. Our transcriptome analyses support a cascade hypothesis in which dysregulation of genes on HSA21 is likely the first genome-level disturbance and gene expression changes on other chromosomes follow quickly thereafter. Indeed, HSA21 genes were already robustly upregulated compared to other chromosomes in the youngest fetal DS samples analyzed in our study, while changes in other regions of the genome increase with age (Figure S3). Moreover, we found that the temporal dynamics of gene module disruptions track the time periods relevant to specific developmental processes. For example, changes in modules 8, 9, 43, and 47 appear during late fetal development and the first several years of postnatal development (Figures 2 and 7), a time in development that coincides with dramatic upregulation of oligodendrocyte/myelination genes (Kang et al., 2011) and rapid expansion of oligodendrocytes in the human brain (Yeung et al., 2014). The record of these expression changes can now be used for the design and application of therapeutics tailored to particular biological process and brain regions at relevant developmental periods.

Myelination is one of the most prolonged neurodevelopmental processes, continuing until the third decade of life (Benes et al., 1994; Flechsig, 1901; Miller et al., 2012; Yakovlev and Lecours, 1967). Notably, human studies have shown that development and maturation of the white matter correlates with increased motor skills and cognitive functions (Casey et al., 2000; Gibson, 1991; Nagy et al., 2004; Paus et al., 1999; Schmithorst et al., 2005). The present results clearly show a profound deficit in white matter maturation in individuals with DS during infancy and adolescence in DFC, a brain region of late myelination that performs a critical role in the organization of behavioral, linguistic, and cognitive functions (Fuster, 2002; Makinodan et al., 2012). Recent evidence in animal models indicates that ongoing myelin remodeling may be important for learning, behavior, and cognition throughout adulthood (Liu et al., 2012; McKenzie et al., 2014). This is in agreement both with previous studies showing that DS children manifest learning and memory problems in late infancy, which often worsen in adolescence (Koo et al., 1992; Lanfranchi et al., 2010), and with postmortem studies that show reduced myelin content (Ábrahám et al., 2012; Wisniewski, 1990; Wisniewski and Schmidt-Sidor, 1989) and fewer oligodendrocytes in DS striatum (Karlsen and Pakkenberg, 2011).

Alterations in white matter or myelin components also may play a role in neuropathology in the aging DS brain with early-onset Alzheimer's-like pathology (Powell et al., 2014). In addition, adults with DS have higher incidence of dementia (Sheehan et al., 2014). While triplication of APP is likely at the root of AD neuropathology in DS, our results raise the intriguing possibility that abnormalities in oligodendrocytes and myelin might contribute to early onset of Alzheimer's-like pathology in DS. Consistent with this possibility, disturbances in myelin have been associated with an increased rate of AD progression, and by-products of homeostatic myelin maintenance can pro-

mote the formation of amyloid plaques (Bartzokis, 2007, 2011). Characterizing the axon-oligodendrocyte interactions in DS throughout development and aging will thus be an important topic of future work.

The concordance between the human DS and Ts65Dn mouse samples at the gene, protein, and cellular levels clearly demonstrates the value of the Ts65Dn mouse in reflecting the cellular and functional consequences of trisomy 21. Our finding that the Ts65Dn white matter phenotype mirrors that occurring in the human DS brain so robustly suggests that it will be a good model to identify neuronal cues that influence the onset and completion of myelination. Both intrinsic and extrinsic factors have been shown to influence myelination. For example, recent studies have shown that electrical activity drives myelination (Gibson et al., 2014; Ishibashi et al., 2006; Wake et al., 2011) and that synaptogenesis and myelination are co-regulated. However, we also show that myelin abnormalities in DS are at least in part due to a cell-autonomous phenomenon in oligodendrocyte development. Teasing out the relative contributions of cell-autonomous effects and neuron-glial signaling, or other cell-extrinsic mechanisms, will be an important goal of future work. These and other queries can now be approached using the developmental expression profiling and multi-species analysis presented here.

In summary, our findings indicate that strategies to enhance myelination may serve as therapeutic targets to attenuate the cognitive and neurological symptoms of DS. Our results also implicate spatiotemporal disturbances in other molecular pathways in DS brain, and they provide a powerful dataset for further computational and functional analyses. We anticipate that the resources provided by this study will inspire and facilitate future studies of the mechanistic basis for impaired neural development in DS and other cognitive disorders, while also lending insight into the genetic and transcriptional underpinnings of previously described DS phenotypes and the relevance of mouse model studies to the human disease.

EXPERIMENTAL PROCEDURES

Human Tissue

This study was conducted using de-identified postmortem human brain specimens from tissue collections at the Department of Neuroscience, Yale School of Medicine; the University of Maryland Brain and Tissue Bank; Brigham and Women's Hospital Pathology Department; and Boston University Pathology Department. Appropriate informed consent was obtained and all available non-identifying information was recorded for each specimen. The ages of specimens, sex, ethnicity, postmortem interval (PMI), RNA integrity number (RIN), and dissection protocol are detailed Tables S1 and S2 and the Supplemental Experimental Procedures. Details of the brain regions analyzed and the dissection technique are detailed in Tables S1 and S2 and the Supplemental Experimental Procedures.

Transcriptome Analyses

Full detailed procedures for RNA isolation and cDNA synthesis can be found in the Supplemental Experimental Procedures and were as previously described (Kang et al., 2011). Affymetrix Human 1.0 ST arrays and the Affymetrix GeneChip platform were used to obtain transcriptome data, as described in the Supplemental Experimental Procedures. Data normalization, quality control, and analysis were performed as detailed in the Supplemental Experimental Procedures. Briefly, the Partek Genomics Suite was used for data normalization and to determine gene level intensities. The expression level

of a gene (transcript cluster) was estimated using the median of all exons within the gene.

Principal component analysis was applied to visualize the relatedness of DS and their matched control samples. A paired t test was used to identify DEX genes between paired DS and matched control samples during all development periods. FDR-adjusted p value < 0.1 was used as a cutoff. Signed co-expression networks were built using the WGCNA package in R (Zhang and Horvath, 2005). Modules were generated by hybrid dynamic tree-cutting. For DEX genes and co-expression modules, functional enrichment was assessed using the Database for Annotation, Visualization and Integrated Discovery (DAVID) Bioinformatics Resource 6.7 (https://david.ncifcrf.gov).

For ddPCR, the same human tissue RNA samples used for exon arrays were used for cDNA synthesis.

Mice, Tissue Culture, and Relevant Procedures

Ts65Dn (RRID: MGI_2178111) and euploid control B6EiC3 mice were generated by backcrossing Ts65Dn females to B6EiC3Sn.BLiAF1/J F1 hybrid (B6EiC3) males. The qPCR genotyping was performed on genomic DNA extracted from tail tips (Chakrabarti et al., 2007). All procedures regarding the care and death of these animals were approved by the Institutional Animal Care and Use Committee of Boston University School of Medicine, in accordance with the NIH Guide for the Care and Use of Laboratory Animals. For procedures relevant to all animal studies, including histology, electron microscopy, image analysis, electrophysiology, immunopanning, oligodendrocyte cultures, and immunoblotting, refer to the Supplemental Experimental Procedures.

ACCESSION NUMBERS

The accession number for all transcriptome data reported in this paper is GEO: GSE59630.

SUPPLEMENTAL INFORMATION

Supplemental Information includes Supplemental Experimental Procedures, seven figures, and nine tables and can be found with this article online at http://dx.doi.org/10.1016/j.neuron.2016.01.042.

AUTHOR CONTRIBUTIONS

ACKNOWLEDGMENTS

REFERENCES

Ábrahám, H., Vincze, A., Veszprémi, B., Kravják, A., Gömöri, É., Kovács, G.G., and Seress, L. (2012). Impaired myelination of the human hippocampal formation in Down syndrome. Int. J. Dev. Neurosci. 30, 147–158.

Ang, E.S., Jr., Haydar, T.F., Gluncic, V., and Rakic, P. (2003). Four-dimensional migratory coordinates of GABAergic interneurons in the developing mouse cortex. J. Neurosci. 23, 5805–5815.

Bahn, S., Mimmack, M., Ryan, M., Caldwell, M.A., Jauniaux, E., Starkey, M., Svendsen, C.N., and Emson, P. (2002). Neuronal target genes of the neuron-restrictive silencer factor in neurospheres derived from fetuses with Down's syndrome: a gene expression study. Lancet 359, 310–315.

Bartzokis, G. (2007). Acetylcholinesterase inhibitors may improve myelin integrity. Biol. Psychiatry 62, 294–301.

Bartzokis, G. (2011). Alzheimer's disease as homeostatic responses to age-related myelin breakdown. Neurobiol. Aging 32, 1341–1371.

Benes, F.M., Turtle, M., Khan, Y., and Farol, P. (1994). Myelination of a key relay zone in the hippocampal formation occurs in the human brain during childhood, adolescence, and adulthood. Arch. Gen. Psychiatry 51, 477–484.

Canfield, M.A., Honein, M.A., Yuskiv, N., Xing, J., Mai, C.T., Collins, J.S., Devine, O., Petrini, J., Ramadhani, T.A., Hobbs, C.A., and Kirby, R.S. (2006). National estimates and race/ethnic-specific variation of selected birth defects in the United States, 1999-2001. Birth Defects Res. A Clin. Mol. Teratol. 76, 747–756.

Casey, B.J., Giedd, J.N., and Thomas, K.M. (2000). Structural and functional brain development and its relation to cognitive development. Biol. Psychol. 54, 241–257.

Chakrabarti, L., Galdzicki, Z., and Haydar, T.F. (2007). Defects in embryonic neurogenesis and initial synapse formation in the forebrain of the Ts65Dn mouse model of Down syndrome. J. Neurosci. 27, 11483–11495.

Chakrabarti, L., Best, T.K., Cramer, N.P., Carney, R.S., Isaac, J.T., Galdzicki, Z., and Haydar, T.F. (2010). Olig1 and Olig2 triplication causes developmental brain defects in Down syndrome. Nat. Neurosci. 13, 927–934.

Cramer, N.P., Xu, X., Haydar, T.F., and Galdzicki, Z. (2015). Altered intrinsic and network properties of neocortical neurons in the Ts65Dn mouse model of Down syndrome. Physiol. Rep. 3, 1–12.

Flechsig, P. (1901). Developmental (myelogenetic) localisation of the cerebral cortex in the human subject. Lancet 2, 1027–1030.

Fuster, J.M. (2002). Frontal lobe and cognitive development. J. Neurocytol. 31, 373–385.

Gibson, K.R. (1991). Myelination and behavioral development: a comparative perspective on questions of neoteny, altriciality and intelligence. In Brain Maturation and Cognitive Development: Comparative and Cross Cultural Perspectives, K.R. Gibson and A. Petersen, eds. (Aldine de Gruyter).

Gibson, E.M., Purger, D., Mount, C.W., Goldstein, A.K., Lin, G.L., Wood, L.S., Inema, I., Miller, S.E., Bieri, G., Zuchero, J.B., et al. (2014). Neuronal activity promotes oligodendrogenesis and adaptive myelination in the mammalian brain. Science 344, 1252304.

Golden, J.A., and Hyman, B.T. (1994). Development of the superior temporal neocortex is anomalous in trisomy 21. J. Neuropathol. Exp. Neurol. 53, 513–520.

Hartley, D., Blumenthal, T., Carrillo, M., DiPaolo, G., Esralew, L., Gardiner, K., Granholm, A.C., Iqbal, K., Krams, M., Lemere, C., et al. (2015). Down syndrome and Alzheimer's disease: common pathways, common goals. Alzheimers Dement. 11, 700–709.

Haydar, T.F., and Reeves, R.H. (2012). Trisomy 21 and early brain development. Trends Neurosci. 35, 81–91.

Hyde, L.A., Frisone, D.F., and Crnic, L.S. (2001). Ts65Dn mice, a model for Down syndrome, have deficits in context discrimination learning suggesting impaired hippocampal function. Behav. Brain Res. *118*, 53–60.

Ishibashi, T., Dakin, K.A., Stevens, B., Lee, P.R., Kozlov, S.V., Stewart, C.L., and Fields, R.D. (2006). Astrocytes promote myelination in response to electrical impulses. Neuron *49*, 823–832.

Kang, H.J., Kawasawa, Y.I., Cheng, F., Zhu, Y., Xu, X., Li, M., Sousa, A.M., Pletikos, M., Meyer, K.A., Sedmak, G., et al. (2011). Spatio-temporal transcriptome of the human brain. Nature *478*, 483–489.

Kaplan, M.R., Cho, M.H., Ullian, E.M., Isom, L.L., Levinson, S.R., and Barres, B.A. (2001). Differential control of clustering of the sodium channels Na(v)1.2 and Na(v)1.6 at developing CNS nodes of Ranvier. Neuron *30*, 105–119.

Karlsen, A.S., and Pakkenberg, B. (2011). Total numbers of neurons and glial cells in cortex and basal ganglia of aged brains with Down syndrome–a stereological study. Cereb. Cortex *21*, 2519–2524.

Kleschevnikov, A.M., Belichenko, P.V., Villar, A.J., Epstein, C.J., Malenka, R.C., and Mobley, W.C. (2004). Hippocampal long-term potentiation suppressed by increased inhibition in the Ts65Dn mouse, a genetic model of Down syndrome. J. Neurosci. *24*, 8153–8160.

Koo, B.K., Blaser, S., Harwood-Nash, D., Becker, L.E., and Murphy, E.G. (1992). Magnetic resonance imaging evaluation of delayed myelination in Down syndrome: a case report and review of the literature. J. Child Neurol. *7*, 417–421.

Lanfranchi, S., Jerman, O., Dal Pont, E., Alberti, A., and Vianello, R. (2010). Executive function in adolescents with Down Syndrome. J. Intellect. Disabil. Res. *54*, 308–319.

Larsen, K.B., Laursen, H., Graem, N., Samuelsen, G.B., Bogdanovic, N., and Pakkenberg, B. (2008). Reduced cell number in the neocortical part of the human fetal brain in Down syndrome. Ann. Anat. *190*, 421–427.

Letourneau, A., Santoni, F.A., Bonilla, X., Sailani, M.R., Gonzalez, D., Kind, J., Chevalier, C., Thurman, R., Sandstrom, R.S., Hibaoui, Y., et al. (2014). Domains of genome-wide gene expression dysregulation in Down's syndrome. Nature *508*, 345–350.

Liu, J., Dietz, K., DeLoyht, J.M., Pedre, X., Kelkar, D., Kaur, J., Vialou, V., Lobo, M.K., Dietz, D.M., Nestler, E.J., et al. (2012). Impaired adult myelination in the prefrontal cortex of socially isolated mice. Nat. Neurosci. *15*, 1621–1623.

Lockstone, H.E., Harris, L.W., Swatton, J.E., Wayland, M.T., Holland, A.J., and Bahn, S. (2007). Gene expression profiling in the adult Down syndrome brain. Genomics *90*, 647–660.

Lott, I.T. (2012). Neurological phenotypes for Down syndrome across the life span. Prog. Brain Res. *197*, 101–121.

Makinodan, M., Rosen, K.M., Ito, S., and Corfas, G. (2012). A critical period for social experience-dependent oligodendrocyte maturation and myelination. Science *337*, 1357–1360.

Mao, R., Zielke, C.L., Zielke, H.R., and Pevsner, J. (2003). Global up-regulation of chromosome 21 gene expression in the developing Down syndrome brain. Genomics *81*, 457–467.

Mao, R., Wang, X., Spitznagel, E.L., Jr., Frelin, L.P., Ting, J.C., Ding, H., Kim, J.W., Ruczinski, I., Downey, T.J., and Pevsner, J. (2005). Primary and secondary transcriptional effects in the developing human Down syndrome brain and heart. Genome Biol. *6*, R107.

McKenzie, I.A., Ohayon, D., Li, H., de Faria, J.P., Emery, B., Tohyama, K., and Richardson, W.D. (2014). Motor skill learning requires active central myelination. Science *346*, 318–322.

Miller, D.J., Duka, T., Stimpson, C.D., Schapiro, S.J., Baze, W.B., McArthur, M.J., Fobbs, A.J., Sousa, A.M., Sestan, N., Wildman, D.E., et al. (2012). Prolonged myelination in human neocortical evolution. Proc. Natl. Acad. Sci. USA *109*, 16480–16485.

Mitchell, A.C., and Mirnics, K. (2012). Gene expression profiling of the brain: pondering facts and fiction. Neurobiol. Dis. *45*, 3–7.

Nagy, Z., Westerberg, H., and Klingberg, T. (2004). Maturation of white matter is associated with the development of cognitive functions during childhood. J. Cogn. Neurosci. *16*, 1227–1233.

Paus, T., Zijdenbos, A., Worsley, K., Collins, D.L., Blumenthal, J., Giedd, J.N., Rapoport, J.L., and Evans, A.C. (1999). Structural maturation of neural pathways in children and adolescents: in vivo study. Science *283*, 1908–1911.

Powell, D., Caban-Holt, A., Jicha, G., Robertson, W., Davis, R., Gold, B.T., Schmitt, F.A., and Head, E. (2014). Frontal white matter integrity in adults with Down syndrome with and without dementia. Neurobiol. Aging *35*, 1562–1569.

Rasband, M.N., Peles, E., Trimmer, J.S., Levinson, S.R., Lux, S.E., and Shrager, P. (1999). Dependence of nodal sodium channel clustering on paranodal axoglial contact in the developing CNS. J. Neurosci. *19*, 7516–7528.

Rueda, N., Flórez, J., and Martínez-Cué, C. (2012). Mouse models of Down syndrome as a tool to unravel the causes of mental disabilities. Neural Plast. *2012*, 584071.

Sahún, I., Marechal, D., Pereira, P.L., Nalesso, V., Gruart, A., Garcia, J.M., Antonarakis, S.E., Dierssen, M., and Herault, Y. (2014). Cognition and hippocampal plasticity in the mouse is altered by monosomy of a genomic region implicated in Down syndrome. Genetics *197*, 899–912.

Schain, A.J., Hill, R.A., and Grutzendler, J. (2014). Label-free in vivo imaging of myelinated axons in health and disease with spectral confocal reflectance microscopy. Nat. Med. *20*, 443–449.

Schmithorst, V.J., Wilke, M., Dardzinski, B.J., and Holland, S.K. (2005). Cognitive functions correlate with white matter architecture in a normal pediatric population: a diffusion tensor MRI study. Hum. Brain Mapp. *26*, 139–147.

Sheehan, R., Ali, A., and Hassiotis, A. (2014). Dementia in intellectual disability. Curr. Opin. Psychiatry *27*, 143–148.

Siarey, R.J., Stoll, J., Rapoport, S.I., and Galdzicki, Z. (1997). Altered long-term potentiation in the young and old Ts65Dn mouse, a model for Down Syndrome. Neuropharmacology *36*, 1549–1554.

Siarey, R.J., Carlson, E.J., Epstein, C.J., Balbo, A., Rapoport, S.I., and Galdzicki, Z. (1999). Increased synaptic depression in the Ts65Dn mouse, a model for mental retardation in Down syndrome. Neuropharmacology *38*, 1917–1920.

State, M.W., and Geschwind, D.H. (2015). Leveraging genetics and genomics to define the causes of mental illness. Biol. Psychiatry *77*, 3–5.

Tanaka, H., Ma, J., Tanaka, K.F., Takao, K., Komada, M., Tanda, K., Suzuki, A., Ishibashi, T., Baba, H., Isa, T., et al. (2009). Mice with altered myelin proteolipid protein gene expression display cognitive deficits accompanied by abnormal neuron-glia interactions and decreased conduction velocities. J. Neurosci. *29*, 8363–8371.

Tebbenkamp, A.T., Willsey, A.J., State, M.W., and Sestan, N. (2014). The developmental transcriptome of the human brain: implications for neurodevelopmental disorders. Curr. Opin. Neurol. *27*, 149–156.

Thaxton, C., Pillai, A.M., Pribisko, A.L., Labasque, M., Dupree, J.L., Faivre-Sarrailh, C., and Bhat, M.A. (2010). In vivo deletion of immunoglobulin domains 5 and 6 in neurofascin (Nfasc) reveals domain-specific requirements in myelinated axons. J. Neurosci. *30*, 4868–4876.

Tyler, W.A., and Haydar, T.F. (2013). Multiplex genetic fate mapping reveals a novel route of neocortical neurogenesis, which is altered in the Ts65Dn mouse model of Down syndrome. J. Neurosci. *33*, 5106–5119.

Wake, H., Lee, P.R., and Fields, R.D. (2011). Control of local protein synthesis and initial events in myelination by action potentials. Science *333*, 1647–1651.

Wang, X., Zhao, Y., Zhang, X., Badie, H., Zhou, Y., Mu, Y., Loo, L.S., Cai, L., Thompson, R.C., Yang, B., et al. (2013). Loss of sorting nexin 27 contributes to excitatory synaptic dysfunction by modulating glutamate receptor recycling in Down's syndrome. Nat. Med. *19*, 473–480.

Wedeen, V.J., Rosene, D.L., Wang, R., Dai, G., Mortazavi, F., Hagmann, P., Kaas, J.H., and Tseng, W.Y. (2012). The geometric structure of the brain fiber pathways. Science *335*, 1628–1634.

Wisniewski, K.E. (1990). Down syndrome children often have brain with maturation delay, retardation of growth, and cortical dysgenesis. Am. J. Med. Genet. Suppl. *7*, 274–281.

Wisniewski, K.E., and Schmidt-Sidor, B. (1989). Postnatal delay of myelin formation in brains from Down syndrome infants and children. Clin. Neuropathol. *8*, 55–62.

Yakovlev, P.I., and Lecours, A. (1967). The myelogenetic cycles of regional maturation of the brain. In Regional Development of the Brain in Early Life, A. Minkowski, ed. (Oxford: Blackwell Science).

Yeung, M.S., Zdunek, S., Bergmann, O., Bernard, S., Salehpour, M., Alkass, K., Perl, S., Tisdale, J., Possnert, G., Brundin, L., et al. (2014). Dynamics of oligodendrocyte generation and myelination in the human brain. Cell *159*, 766–774.

Yoshida, K., Toki, T., Okuno, Y., Kanezaki, R., Shiraishi, Y., Sato-Otsubo, A., Sanada, M., Park, M.J., Terui, K., Suzuki, H., et al. (2013). The landscape of somatic mutations in Down syndrome-related myeloid disorders. Nat. Genet. *45*, 1293–1299.

Zampieri, B.L., Biselli-Périco, J.M., de Souza, J.E., Bürger, M.C., Silva Júnior, W.A., Goloni-Bertollo, E.M., and Pavarino, E.C. (2014). Altered expression of immune-related genes in children with Down syndrome. PLoS ONE *9*, e107218.

Zhang, B., and Horvath, S. (2005). A general framework for weighted gene co-expression network analysis. Stat. Appl. Genet. Mol. Biol. *4*, Article17.

Zhang, Y., Chen, K., Sloan, S.A., Bennett, M.L., Scholze, A.R., O'Keeffe, S., Phatnani, H.P., Guarnieri, P., Caneda, C., Ruderisch, N., et al. (2014). An RNA-sequencing transcriptome and splicing database of glia, neurons, and vascular cells of the cerebral cortex. J. Neurosci. *34*, 11929–11947.